Geophysical Research Letters

RESEARCH LETTER
10.1029/2025GL118290

Direct Observations of Acceleration of Planetary Ions From Mars' Ionosphere Through Magnetic Reconnection When IMF Rotates

Rentong Lin[1,2,3], Shiyong Huang[3], Yuming Wang[1,2], Qiyang Xiong[3], Zhigang Yuan[3], Honghong Wu[3], Kui Jiang[3], Guoqiang Wang[4], Yutian Chi[1,2], and Tielong Zhang[4,5]

[1]National Key Laboratory of Deep Space Exploration/School of Earth and Space Sciences, University of Science and Technology of China, Hefei, China, [2]CAS Center for Excellence in Comparative Planetology/CAS Key Laboratory of Geospace Environment/Mengcheng National Geophysical Observatory, University of Science and Technology of China, Hefei, China, [3]School of Earth and Space Science and Technology, Wuhan University, Wuhan, China, [4]Institute of Space Science and Applied Technology, Harbin Institute of Technology, Shenzhen, China, [5]Space Research Institute, Austrian Academy of Sciences, Graz, Austria

Abstract Mars lacks an intrinsic global magnetic field but possesses crustal magnetic anomalies and an atmosphere. Mars' ionosphere, resulted from interactions between Mars' atmosphere and solar radiation, directly interacts with solar wind and interplanetary magnetic field (IMF). However, the mechanisms governing ion acceleration and escape from Mars' ionosphere remain incompletely understood. By analyzing simultaneous observations from MAVEN and Tianwen-1 missions, we present observational evidence of magnetic reconnection events in Mars' dayside upper ionosphere above weak crustal field region during IMF rotation, accompanied by acceleration of ionospheric ions. The explosive escape flux exceeds the average plume and tailward escape flux by an order of magnitude and is comparable to that of reconnection processes above strong crustal field regions. Our results provide evidence that IMF rotation-triggered magnetic reconnection constitutes a significant pathway for ion escape from Mars, offering new insights into planet's atmospheric evolution and potential mechanisms for early water loss on Mars.

Plain Language Summary Mars, unlike Earth, doesn't have a strong global magnetic field. Instead, it has patchy magnetic spots in its crust. Solar radiation creates a protective layer around Mars, but ions from Mars' atmosphere still escape into space, contributing to the planet's water loss. Scientists have long wondered exactly how these ions get sped up and eject. By analyzing data from NASA's MAVEN and China's Tianwen-1 missions we spotted a rare event at Mars. We saw the sun's magnetic field suddenly twist, which triggered a process called magnetic reconnection near Mars. This is where magnetic fields snap and reconnect, releasing energy like a rubber band. During this event, protons and oxygen ions from Mars' atmosphere were dramatically accelerated. This created powerful jets shooting ions away from Mars. The explosive ion escape flux was larger than during steady solar wind conditions when reconnection occurs. This implies that magnetic reconnection, especially when the sun's magnetic field changes, could be a significant driver of Mars' atmospheric loss. In the planet's early history, when the sun was more active, such events might have played an oversized role in stripping away water. Understanding this helps piece together how Mars became the dry world we see today.

Key Points:

- Direct observation of magnetic reconnection in dayside Mars' ionosphere above weak crustal field regions, linking interplanetary magnetic field (IMF) rotation to ion escape
- The transient ion escape flux in this case is an order larger than that of plume/tailward escape and rival that above strong crustal fields
- IMF-triggered reconnection should be significant for historical atmospheric loss due to enhanced solar wind pressure and IMF variations

Supporting Information:

Supporting Information may be found in the online version of this article.

Correspondence to:

R. Lin, S. Huang and Y. Wang,
rentonglin@ustc.edu.cn;
shiyonghuang@whu.edu.cn;
ymwang@ustc.edu.cn

Citation:

Lin, R., Huang, S., Wang, Y., Xiong, Q., Yuan, Z., Wu, H., et al. (2025). Direct observations of acceleration of planetary ions from Mars' ionosphere through magnetic reconnection when IMF rotates. *Geophysical Research Letters*, *52*, e2025GL118290. https://doi.org/10.1029/2025GL118290

Received 21 JUL 2025
Accepted 5 NOV 2025

1. Introduction

Mars lacks a global intrinsic magnetic field, but strong crustal magnetic anomalies were discovered by the Mars Global Surveyor orbiter (Acuña et al., 1998). The Martian atmosphere is partially ionized by solar radiation, forming an ionosphere that deflects the solar wind and interplanetary magnetic field (IMF), thereby generating induced currents and creating an induced magnetosphere (Dubinin et al., 2013). Crustal magnetic fields can similarly deflect the solar wind and IMF, forming mini-magnetospheres (Fan et al., 2023) analogous to Earth's magnetosphere. The Martian ionosphere contains a high density of low-energy thermal ions, which can be accelerated through magnetospheric dynamical processes when entering the magnetosphere or magnetosheath. These processes include solar wind pickup (e.g., Dong et al., 2015; Ma et al., 2023), wave-particle interactions (e.g., Collinson et al., 2018; Fowler et al., 2021), and magnetic reconnection (e.g., Harada et al., 2015; Wang et al., 2021; Ye et al., 2024), ultimately leading to ion escape into the magnetotail or interplanetary space.

However, the mechanisms governing ion acceleration and escape from the ionosphere into the magnetosphere remain incompletely understood and constitute a critical question.

Magnetic reconnection is a fundamental process in astrophysical and space plasmas, capable of altering magnetic field topology and efficiently converting magnetic energy into thermal and kinetic energy (e.g., Biskamp, 1986; Deng & Matsumoto, 2001; Eastwood et al., 2008, 2015; Huang et al., 2018, 2021; Jiang et al., 2022; Vasyliunas, 1975; Xiong et al., 2023). This phenomenon has been observed at the dayside magnetopause in Earth's magnetosphere (Burch & Phan, 2016; Phan et al., 2000), as well as at Mars' induced-magnetopause (Wang et al., 2021) and mini-magnetopause (Lin, Huang, Yuan, Jiang, Wu, & Xiong, 2024). Reconnection events have also been documented across Mars' crustal field regions (Chen et al., 2023; Harada et al., 2018; Lin, Huang, Yuan, Jiang, Wu, & Xiong, 2024; Lin, Huang, Yuan, Jiang, Xu, et al., 2024; Ye et al., 2024) and within its induced magnetosphere/magnetotail (Harada et al., 2015; Wang et al., 2021). Ions from Mars can be accelerated through reconnection (Harada et al., 2015; Wang et al., 2021; Ye et al., 2024), while solar wind plasma can penetrate the Mars' magnetosphere through reconnection regions (Lin, Huang, Yuan, Jiang, Wu, & Xiong, 2024; Zhang et al., 2023). Cravens et al. (2020) evaluated the role of magnetic reconnection in Mars' dayside ionosphere under collisional conditions, and found that the efficiency of magnetic reconnection is reduced by collisions at lower altitudes (below about 300 km) in the Mars' ionosphere. However, direct evidence of magnetic reconnection in the dayside Mars' upper ionosphere above weak crustal field regions, a potential contributor to ionospheric escape, remains unexplored.

Utilizing simultaneous magnetic field and plasma measurements from the Mars Atmosphere and Volatile Evolution (MAVEN) and Tianwen-1 missions, we report novel observations of magnetic reconnection in dayside Mars' upper ionosphere during IMF rotation events. Our findings demonstrate the acceleration of protons and oxygen ions from the Mars' upper ionosphere during reconnection. The estimated escape flux in this event exceeds the average values of plume and tailward escape by an order of magnitude and comparable to those during reconnection events above strong crustal fields. These results suggest that magnetic reconnection may constitute a significant pathway for ion escape from the Mars' upper ionosphere during periods of IMF variation.

2. Data and Instruments

The data used in this study were from the MAVEN mission and the Tianwen-1 mission. The MAVEN measurements were particularly from Magnetometer (MAG; Connerney et al., 2015), Solar Wind Electron Analyzer (SWEA; Mitchell et al., 2016) and Supra-Thermal And Thermal Ion Composition (STATIC; McFadden et al., 2015). The Tianwen-1 measurements were from the Mars Orbiter Magnetometer (MOMAG; Liu et al., 2020; Wang et al., 2023). MOMAG and MAG provide 3D magnetic fields with a cadence of 32 vectors s^{-1}. The reliability of MOMAG has been verified by Zou et al. (2023) and Wang et al. (2024). The absolute vector accuracy of data from MAG is 0.05% (Connerney et al., 2015). SWEA provides an electron energy spectrogram and pitch angle distribution at a temporal resolution of 2 s. STATIC provides an omni-directional energy spectrogram of ions with a temporal resolution of 4 s and three-dimensional distributions to estimate the bulk flow velocity, available as fast as every 16 s. Note that the ion density and velocity vectors are derived from STATIC measurements.

We employed the methodology developed by Xu et al. (2019) to identify magnetic topology by combining two methods: the identification of electron loss cones and the identification of source regions of superthermal electrons. Ambiguities exist for the loss-cone method on the dayside and for the electron-source method on the nightside. Their combination provides the most accurate and comprehensive topology determination (Xu et al., 2019). Low electron fluxes (loss cones) detected at pitch angles of 0° and/or 180° indicate atmospheric energy absorption and that the magnetic field line intersects the collisional atmosphere on one or both ends (e.g., Brain et al., 2007; Weber et al., 2017). From this, a one-sided loss cone indicates an open field line, whereas a double-sided loss cone indicates a closed field line. The presence of ionospheric photoelectrons traveling parallel and/or antiparallel to the magnetic field implies one or two foot point(s) embedded in the dayside ionosphere. Combining these two methods enables classification as: closed fields (indicating two foot points), open fields (indicating one foot point), or draped fields (indicating zero foot points). Cases not fitting these classifications are considered unknown.

3. Observations

Figure 1 shows an overview of the current sheet crossing event of MAVEN on the dayside of Mars from 02:12–02:32 UT on 7 November 2024. Plasma and magnetic field measurements are shown in Mars-solar-orbital (MSO) coordinates. In MSO coordinates, the X-axis points from Mars toward the sun, the Y-axis points opposite to the direction of the orbital velocity component of Mars perpendicular to the X-axis, and the Z-axis completes the orthogonal coordinate set. As shown in Figure 1b, the orbiter of MAVEN fled outbound on the dayside. The magnetic field component B_y reverses from positive to negative during 02:18:50–02:19:30 UT accompanied by a local minimum in the total magnetic field (~02:19:08 UT, Figure 1c) and a local maximum in the ion density (~02:19:10 UT, Figure 1h), which indicates the crossing of a current sheet (marked by two dashed lines).

Note that there exists an ion composition boundary (ICB) between Mars' ionosphere/induced magnetosphere and magnetosheath: below the ICB, the ion components are mainly composed of ions from Mars (e.g., O^+ and O_2^+ ions), and the ion density decreases with altitude; when moving upward across the boundary, the dominant ion components shift from Mars' ions to solar wind protons, at which point a sharp drop in ion density occurs (e.g., Dubinin et al., 2006). During this outbound process of MAVEN, the observed ion density first gradually decreased and then exhibited a sharp drop (probably ICB). The local ion density maximum was detected just prior to the sharp drop in ion density, and the simultaneous occurrence of the magnetic field minimum and ion density maximum indicates the crossing of a current sheet below the ICB.

Using the methodology developed by Xu et al. (2019), the magnetic topology around the current sheet was identified (Figure 1i). Figures 1j and 1k display energy flux of electrons in regions below the current sheet (02:16:53–02:17:05 UT) and above the current sheet (02:21:53–02:22:05 UT). In regions below the current sheet, features of ionospheric photoelectrons, that is, photoelectron knee (e.g., Shane et al., 2016), Auger peaks (e.g., Mitchell et al., 2000), and flux dropoff near 500 eV (e.g., Liemohn et al., 2003), were detected within the electron distributions along the direction of parallel and antiparallel of the magnetic field (Figure 1j). It suggested that the magnetic topology in regions below the current sheet is closed field. And the electrons distribution above the current sheet showed no features of ionospheric photoelectrons (Figure 1k), indicating that the magnetic topology in regions above the current sheet is draped field. It suggested that the topology of magnetic field changed from closed field to open/draped field when MAVEN crossing the current sheet (Figures 1i–1k).

Figure 2 shows the detailed observations by MAVEN orbiter around the current sheet during 02:17:50–02:20:30 UT and comprehensive evidence for the occurrence of magnetic reconnection. The magnetic field and velocity vectors of ions are transformed from MSO coordinates to local LMN coordinates. The current sheet normal points along N-direction, L-direction is along the anti-parallel magnetic-field direction and $M = N \times L$ is in the out-of-plane ("X-line") direction (Hapgood, 1992). The LMN coordinates are obtained by minimum variance analysis (MVA; e.g., Sonnerup & Scheible, 1998a, 1998b), in which $L = [-0.35, -0.93, 0.10]$, $M = [0.93, -0.34, 0.12]$, and $N = [-0.08, 0.14, 0.99]$ in MSO coordinates using magnetic field measurements in the time interval of 02:18:50–02:19:30 UT. The ratios of the eigenvalues corresponding to the maximum λ_1 and intermediate λ_2 and between the intermediate λ_2 and minimum λ_3 are $\lambda_1/\lambda_2 = 15.53$ and $\lambda_2/\lambda_3 = 27.02$, respectively, indicating that the MVA results are reliable (e.g., Sonnerup & Scheible, 1998a, 1998b). The magnetic field component B_L reverses from negative to positive (Figure 2b). And the component B_M shows a bipolar signature from positive to negative relative to the guide field B_g ($B_g \approx -3.27$ nT, estimated by averaging the magnetic field component B_M from 02:17:50 to 02:18:42 UT and from 02:19:36 to 02:20:30 UT in Figure 2c) in intense plasma flow (enhanced proton and oxygen ion velocity component V_L in Figures 2e–2g). The upstream Alfven speed estimated in the time interval between 02:17:50 and 02:18:50 UT is 5.86 km/s. The mean plasma flow speed in the outflow jets is about 3.49 km/s in the reconnection region, which is lower than the upstream Alfven speed. At approximately 02:19:00 UT, the electron distributions were predominantly concentrated along the direction parallel to the magnetic field (Figure 2l). At 02:19:30 UT, however, the primary direction of the electrons have shifted to the antiparallel direction relative to the magnetic field. During MAVEN's traversal of the current sheet center between 02:19:10 UT and 02:19:22 UT, the observed electron motion was not strictly perpendicular to the magnetic field but exhibited a deflection toward the antiparallel direction. This characteristic is consistent with electron behavior observed by the Magnetospheric Multiscale (MMS) Mission in reconnection events occurring under strong guide fields (Genestreti et al., 2017; Huang et al., 2021). In the presence of a guide field, electrons near the X-line can be both driven along the B_M direction and accelerated along the M-axis by the reconnection electric field (Genestreti et al., 2017). These features are consistent with the Hall magnetic field and plama outflow in

10.1029/2025GL118290

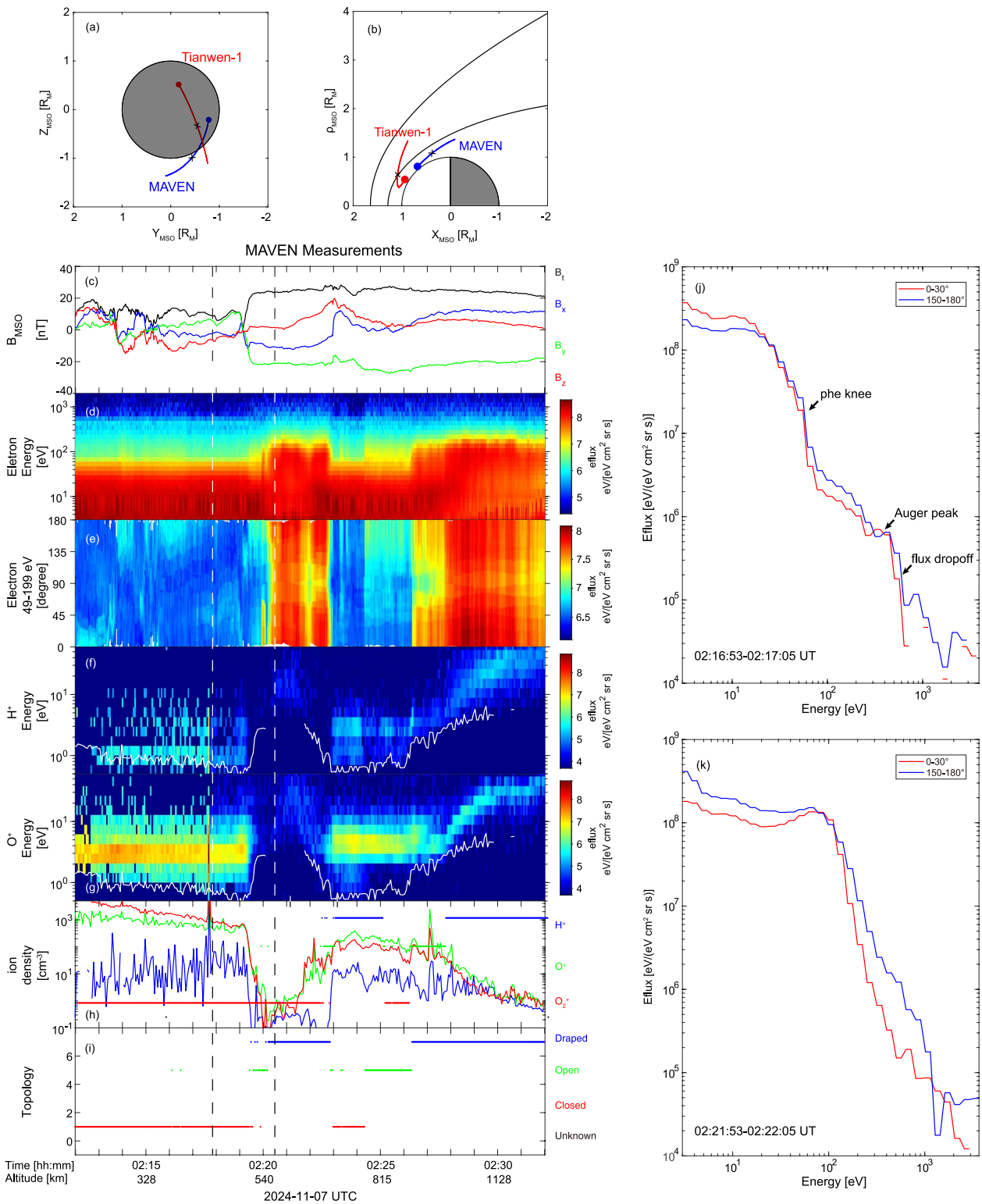

Figure 1.

the ion diffusion region of the Hall reconnection model (e.g., Deng & Matsumoto, 2001; Eastwood et al., 2008; B. U. O. Sonnerup, 1979). Therefore, magnetic reconnection did occur in this current sheet. Note that the fluctuation of velocity of protons in the reconnection region indicated the chaotic motion that probably resulted from the overlap of nonlinear resonances between bounce motion and gyro motion (e.g., Buchner & Zelenyi, 1986, 1989; Liu et al., 2015; Xiong et al., 2024; Zenitani et al., 2013).

The time series of angular spectra of H^+, O^+, and $O_2{}^+$ ions were obtained by STATIC-d1 data product (shown in Figure 3). When the reconnection occurred, the ion flow direction changed toward the L direction, especially in the elevation/theta angle. The ion spectrograms (Figures 2i–2k) and ion angular distribution (Figure 3) suggest that ions were energized in the reconnection region compared to those in the closed field. The enhancement in ion velocity occurred along the L-axis, corresponding to the direction of anti-parallel to Y-axis in the MSO coordinates, with the reconnection region located in the western hemisphere ($Y < 0$; Figure 1a). This indicates that ions were accelerated along the direction of escape from Mars. Besides, the reconnection event was located near the ICB, and ions were accelerated in the direction away from the ICB, indicating that the ions were probably to escape the ionosphere. Under the assumption that all these ions eventually escaped from Mars, the escape flux can be estimated with the ion density and bulk velocity. The estimated escape flux of O^+ ions is approximately 5.44×10^{11} m^{-2} s^{-1}, with an oxygen ion density of 4.01×10^2 cm^{-3} and a bulk velocity of 1.36 km/s. The estimated escape flux of $O_2{}^+$ ions is approximately 4.35×10^{11} m^{-2} s^{-1}. Note that the L direction was out of the field of view (FOV) of STATIC (Figure 3) and the most energetic part of ion distribution might not be captured. This indicates that the ion density and velocity obtained by integrating across various angular and energy channels should be underestimated, and consequently, the contribution to ion escape flux estimated here should also be underestimated.

Magnetic field measurements from MAVEN and Tianwen-1 combined with crustal field models are utilized to determine whether the region traversed by MAVEN is dominant by remanent crustal fields or not. Figure S1 displays magnitude of magnetic field measurements by MAVEN and those of crustal field from G110 model developed by Gao et al. (2021) and from L134 model by Langlais et al. (2019), respectively. After 02:14 UT, the magnetic field intensity observed by MAVEN is significantly larger than those predicted by the G110 model and the L134 model, implying that in the regions traversed by MAVEN, there is no crustal magnetic field or the contribution of the crustal magnetic field is negligible. Figure S1b displays magnitude of magnetic field measurements by Tianwen-1 and those of crustal field from G110 model and the L134 model. The magnetic field intensity observed by Tianwen-1 is significantly larger than those predicted by the G110 model and the L134 model (Figure S1b). This indicates that the magnetic field variations observed by Tianwen-1 are predominantly dominated by changes in the IMF, with negligible contributions from crustal magnetic fields.

Clock angle of the magnetic field is defined as the angle measured from the +Z axis towards the +Y axis within the Y-Z plane in MSO coordinates, ranging from 0° to 360°, which can represent direction of the magnetic field vector within the Y-Z plane. Figure 4a shows the clock angle of the magnetic field observed by both Tianwen-1 and MAVEN. At quasi-steady state, the clock angle of magnetic field in the induced magnetosphere/upper ionosphere above weak crustal field region should be similar to that of the IMF since draping magnetic field originates from the IMF; when the IMF rotates, the magnetic field in the induced magnetosphere/upper ionosphere above weak crustal field region should rotate accordingly within minutes (Modolo et al., 2012; Romanelli et al., 2019), eventually aligning toward a similar direction of the IMF within the Y-Z plane.

A cross-correlation analysis was performed on the magnetic field clock angles observed by Tianwen-1 and MAVEN. This revealed a maximum correlation coefficient 0.77 between these two signals at a time lag of ∼105 s (Figure 4b). The dashed curve in Figure 4c represents the time-shifted clock angle of magnetic field observed by

Figure 1. Overview of the current sheet crossing event on 7 November 2024 during 02:12:00–02:32:00 UT. Orbits of MAVEN and Tianwen-1 (a) in Y-Z plane and (b) in X-ρ plane, where $\rho = \sqrt{y^2 + z^2}$; (c) magnetic field in MSO coordinates; (d) electron spectrogram; (e) pitch angle distribution of electrons (49–199 eV); (f, g) H^+ and O^+ ion spectrogram; (h) ion density; (i) the estimated magnetic field topology; and the energy flux of electrons in the time interval of (j) 02:16:53–02:17:05 UT and (k) 02:21:53–02:22:05 UT, respectively. Black curves in (b) represent the bow shock and induced magnetopause models (Vignes et al., 2000), respectively. The dots represents start of the orbits at 02:12:00 UT. White curves in panel (e, f) represent the electric potential of MAVEN. The dashed lines represent the time interval of the current sheet crossing during 02:17:50–02:20:30 UT. The crosses on blue curves in panel (a, b) represent position of MAVEN at 02:19:00 UT. The crosses on red curves in panel (a, b) represent position of Tianwen-1 at 02:17:15 UT which is 105 s before 02:19:00 UT. The red and blue curves in panel (j, k) represent electron pitch angle within 0–30° and within 150–180°.

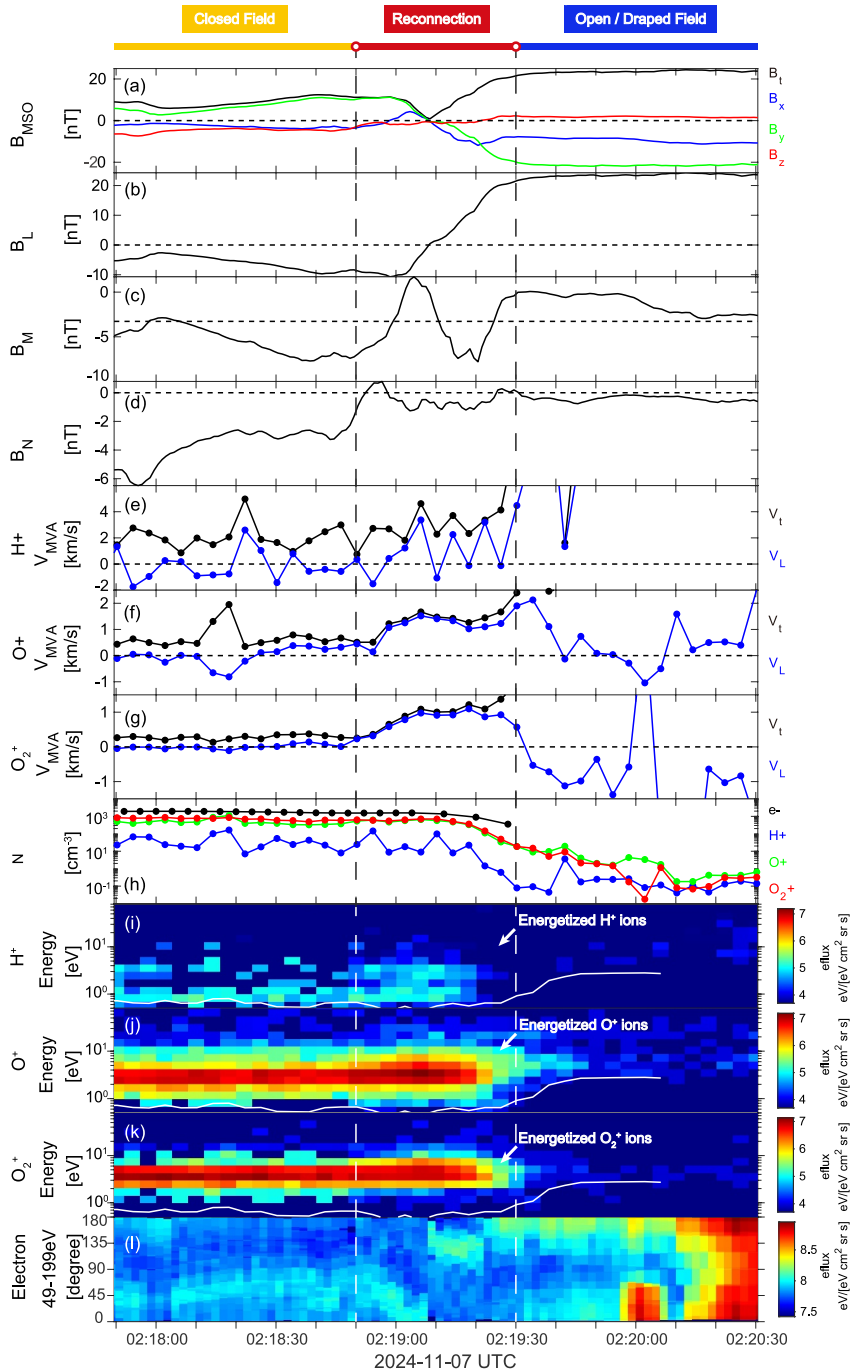

Figure 2. Zoom-in of the current sheet crossing event on 7 November 2024 during 02:17:50–02:20:30 UT. The magnitude and three components of magnetic field (a) in the MSO coordinates; three components of magnetic field in the LMN coordinates, that is, (b) B_L, (c) B_M, (d) B_N; (e–g) velocity component along the L-axis (V_L) of H^+, O^+, and O_2^+ ions in the LMN coordinates, (h) ion and electron density, (i–k) spectrograms of H^+, O^+, and O_2^+ respectively, and (l) pitch angle distribution of electrons (49–199 eV). Vertical dashed lines represent the reconnection region in the time interval of 02:18:50–02:19:30 UT. White curves in panel (i–k) represent the electric potential of MAVEN. It suggests that energization of ions does not result from the variation of electric potential of MAVEN.

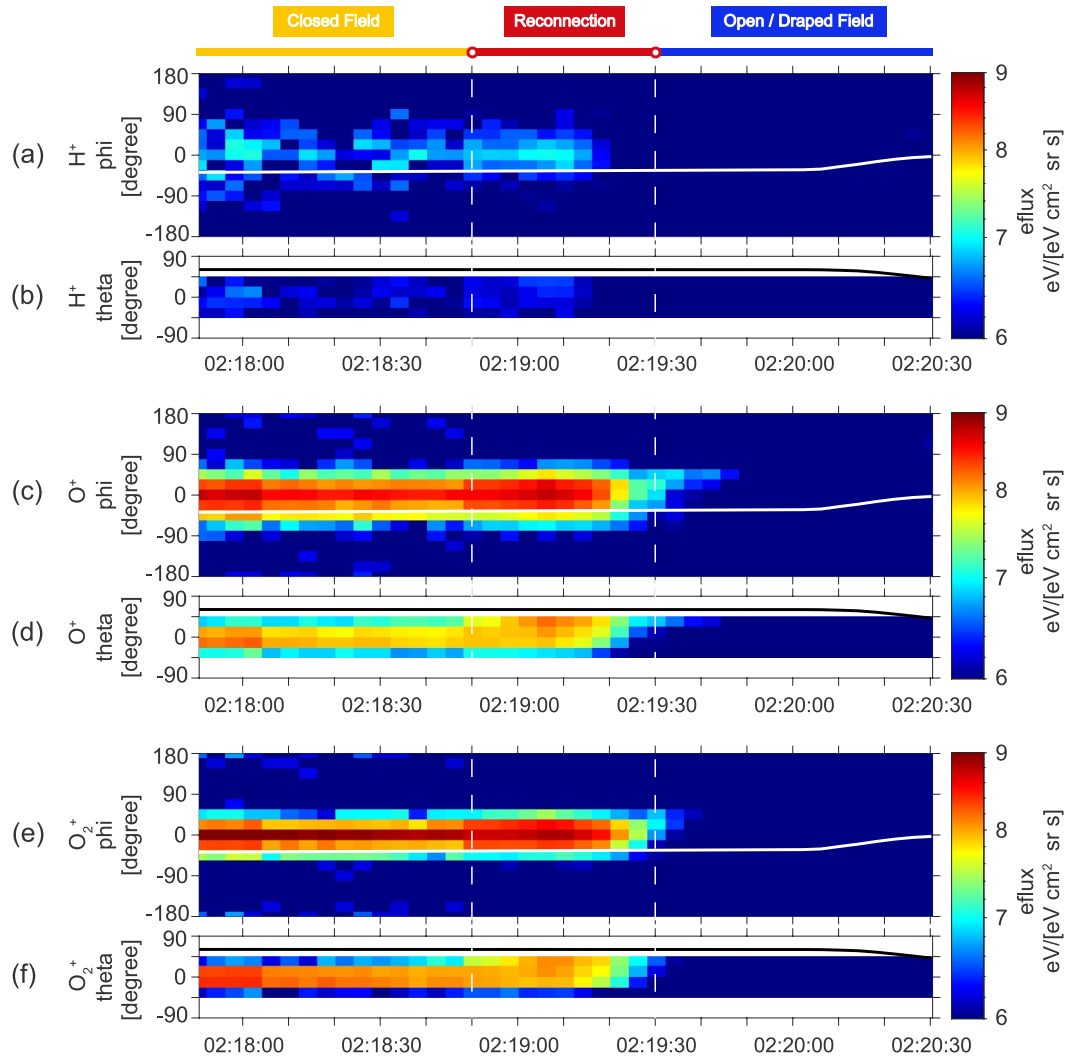

Figure 3. Time series of the ion angular distribution measured by MAVEN on 7 November 2024 during 02:17:50–02:20:30 UT. Angular spectra of H^+ (a) in the STATIC azimuthal/phi angle, and (b) in the STATIC elevation/theta angle; angular spectra of O^+ (c) in the STATIC azimuthal/phi angle, and (d) in the STATIC elevation/theta angle; angular spectra of O_2^+ (e) in the STATIC azimuthal/phi angle, and (f) in the STATIC elevation/theta angle. The solid white/black lines indicate the L directions in the instrument coordinate. The horizontal dashed lines mark the reconnection region.

Tianwen-1. The clock angle of magnetic field observed by MAVEN aligns well with the time-shifted clock angle of magnetic field observed by Tianwen-1. This demonstrates that the dominant directional changes in the magnetic field observed by MAVEN were driven by variations in the IMF direction. It also indicates that the Mars' ionosphere responds rapidly within a few minutes to variation of the IMF.

In this event, the change of clock angle of IMF ranges from ∼90 to 120°. It is known that magnetic reconnection can occur between parallel and anti-parallel magnetic field lines, where the shear angle is 180°. However, there was evidence of low-shear reconnection at Mercury's magnetopause at shear angles <70° (Zomerdijk-Russell et al., 2023). Besides, large shear angle (90–180°) and low-β current sheets, which presumably without reconnection suppression, are commonly formed at Mars (Harada et al., 2020). Thus, It is not necessary for ∼180° shear angle of magnetic field lines to trigger reconnection and the shear angle in this event will not restrict the occurrence of magnetic reconnection.

MAVEN observed a magnetic reconnection event within the Mars' upper ionosphere above weak crustal field region around 02:19 UT. And the moment of this reconnection event exhibited a precise correspondence with that

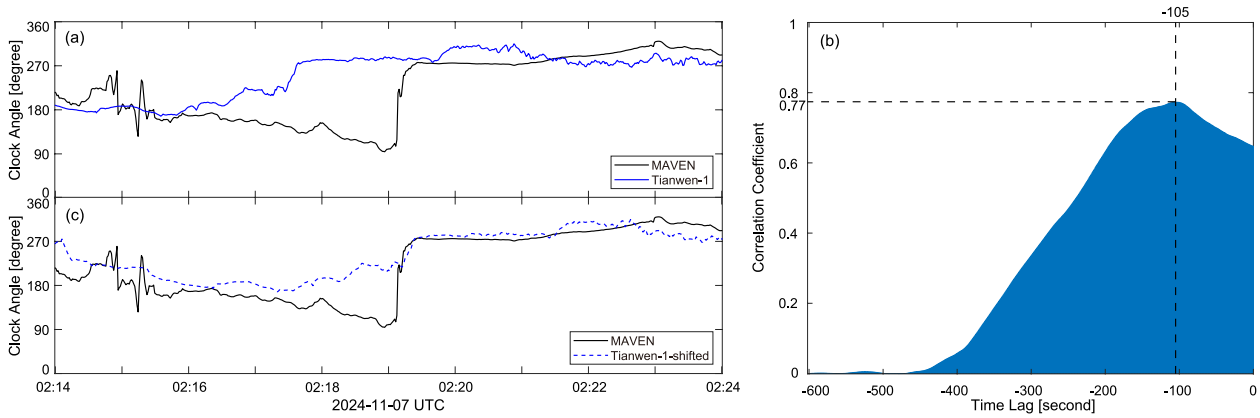

Figure 4. The clock angle of magnetic field measured by Tianwen-1 and MAVEN and the cross-correlation analysis on these two signal. (a) Clock angle of magnetic field measured by MAVEN and Tianwen-1; (b) correlation coefficient with time lags; (c) clock angle of magnetic field measured by MAVEN and clock angle forward-shifted by 105 s of magntic field measured by Tianwen-1. A time delay of less than zero indicates that either the MAVEN measurements are shifted backward in time or the Tianwen-1 measurements are shifted forward in time. Note that a time delay of more than zero is not shown for that it is not physical. It should be noted that positive time delays are not displayed, as a time delay >0 would imply MAVEN measurements precede those of Tianwen-1, which is unphysical. The Blue curves in panel (a, c) represent the clock angle of magnetic field measured by Tianwen-1.

of the IMF directional change observed by Tianwen-1. This indicates that the reconnection event resulted from the IMF rotation. Figure 5 illustartes the idea of the reconnection process when IMF rotates.

4. Discussions

It should be noted that the electron energy spectra and pitch-angle distributions during the first observed draped field period (02:20–02:23 UT) are highly similar to those during the second draped field period (02:28−02:32 UT). During the second draped field period, the ion density of O^+ and $O_2{}^+$ ions decreased and was lower than that of H^+ ions after 02:34 UT (not shown here), indicating that it was the ICB. Since the second draped field region is confirmed to correspond to the ICB, this similarity suggests the first one is also likely a boundary between plasmas in magnetosheath and plasmas from Mars. Analysis of MAVEN's magnetic field and plasma data has confirmed magnetic reconnection occurred before the first observed draped field period, with effective ion acceleration. Additionally, Tianwen-1's magnetic field data revealed a rotation in the IMF direction, and the ICB was observed after reconnection. We thus propose the following mechanism for the first magnetic topology change (02:20–02:23 UT): local plasmas were accelerated by magnetic reconnection and moved to higher altitudes, creating a transient plasma cavity (similar to the scenario of Ye et al., 2024). Subsequently, lower-altitude plasma moved upward driven by pressure gradients to fill this cavity (closed field, 02:23–02:25 UT).

Comparing to established escape paradigms, the escaping flux in this reconnection event (5.44×10^{11} m^{-2} s^{-1}) exceeds that of averaged plume and tailward escape (up to 1.5×10^{10} m^{-2} s^{-1} from Dong et al., 2015) by an order and is comparable to strong crustal-field mass ejections (~4×10^{11} m^{-2} s^{-1} from Ye et al., 2024; ~6×10^{11} m^{-2} s^{-1} from Lin, Huang, Yuan, Jiang, Wu, & Xiong, 2024). It should be noted that the potential ion escape flux in this event may be underestimated due to the limited FOV of STATIC and the estimated value should be regarded as a lower limit. These escape frameworks demonstrate while steady plume and tailward loss dominates background escape processes and crustal reconnection induces localized explosive depletion, IMF-rotation-driven reconnection emerges as a comprehensive transient enhancement mechanism. The historical significance of this phenomenon likely surpasses its current impact, as enhanced solar wind pressure and IMF instability during the young Sun phase (Russell, 2001; Tarduno et al., 2010) may have amplified such events by an order of magnitude throughout Mars' hydrologically active period, potentially establishing weak-field reconnection as the predominant pathway for early water loss. To achieve accurate quantification of cumulative atmospheric depletion across geological timescales, future models must incorporate this IMF-dependent kinetic process. It is also necessary to clarify that magnetic reconnection does not occur continuously but is a transient and explosive process, whereas polar plume and tailward escape presumably occur continuously. Therefore, the estimation of the occurrence rate of magnetic reconnection is an essential step to quantify the contribution of this explosive escape enhancement mechanism to ion escape.

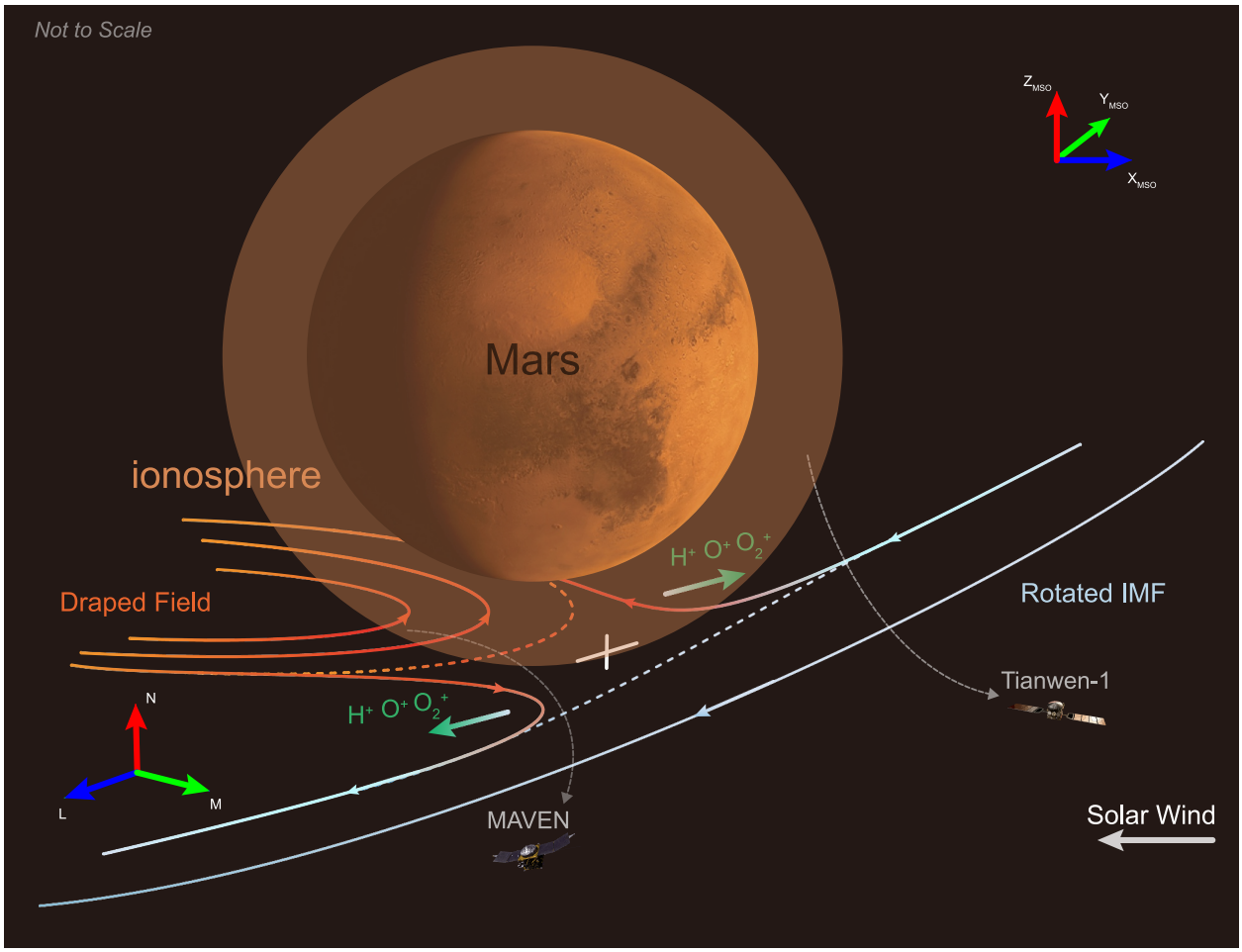

Figure 5. The cartoon of magnetic reconnection in the ionosphere. The orange circle represents the ionosphere. The curves with arrows represent magnetic field lines. The warm curves represent the magnetic field in the ionosphere and the cold ones represent the rotated interplanetary magnetic field (IMF). The dashed warm and clod curves represent the original magnetic field line in the ionosphere and the original IMF before rotating, which reconnects to the other. The dashed white curves with arrowhead represent the orbit of MAVEN and Tianwen-1. The cross represents the reconnection X line. The green arrows represent the plasma flow.

To summarize, we present evidence of a magnetic reconnection event occurring in the Mars' upper ionosphere above weak crustal field region when the IMF rotates. The reconnection process exhibited clear acceleration of ions from Mars' ionosphere away from the planet. Notably, the observed ion escape flux during this event substantially exceeded the characteristic fluxes associated with both solar wind pickup processes and magnetic reconnection within mini-magnetospheres. These findings suggest that magnetic reconnection events in the Mars' upper ionosphere above weak crustal field region, particularly during IMF variations, may serve as a crucial mechanism for converting thermal ion populations in the ionosphere into escaping ion beams, which could be an important channel for ions to be accelerated before escaping from the Mars' ionosphere.

Conflict of Interest

The authors declare no conflicts of interest relevant to this study.

Data Availability Statement

The Tianwen-1 data may be downloaded from the official website of the MOMAG team (http://space.ustc.edu.cn/dreams/tw1_momag/) or applied at CNSA Data Release System (https://moon.bao.ac.cn/web/zhmanager/mars1). The MAVEN data used in this study are publicly available at the website: https://lasp.colorado.edu/maven/sdc/public/data/sci/.

Acknowledgments
We acknowledge the entire Tiannwen-1 and MAVEN teams for data access and support. This work was supported by the National Natural Science Foundation of China (42130204, 42441811). We appreciate the useful discussions with Dr. Wanqiu Feng from University of Science and Technology of China.

References

Acuña, M. H., Connerney, J. E. P., Wasilewski, P., Lin, R. P., Anderson, K. A., Carlson, C. W., et al. (1998). Magnetic field and plasma observations at Mars: Initial results of the Mars global Surveyor mission. *Science*, *279*(5357), 1676–1680. https://doi.org/10.1126/science.279.5357.1676

Biskamp, D. (1986). Magnetic reconnection via current sheets. *Physics of Fluids*, *29*(5), 1520–1531. https://doi.org/10.1063/1.865670

Brain, D., Lillis, R., Mitchell, D., Halekas, J., & Lin, R. (2007). Electron pitch angle distributions as indicators of magnetic field topology near Mars. *Journal of Geophysical Research*, *112*(A9), A09201. https://doi.org/10.1029/2007JA012435

Buchner, J., & Zeleny, L. M. (1986). Deterministic chaos in the dynamics of charged-particles near a magnetic-field reversal. *Physics Letters A*, *118*(8), 395–399. https://doi.org/10.1016/0375-9601(86)90268-9

Buchner, J., & Zelenyi, L. M. (1989). Regular and chaotic charged-particle motion in magnetotail-like field reversals. 1. Basic theory of trapped motion. *Journal of Geophysical Research*, *94*(A9), 11821–11842. https://doi.org/10.1029/JA094ia09p11821

Burch, J. L., & Phan, T. D. (2016). Magnetic reconnection at the dayside magnetopause: Advances with MMS. *Geophysical Research Letters*, *43*(16), 8327–8338. https://doi.org/10.1002/2016GL069787

Chen, G., Huang, C., Zhang, Y., Ge, Y., Du, A., Wang, R., et al. (2023). MAVEN observations of the interloop magnetic reconnections at Mars. *The Astrophysical Journal*, *952*(1), 37. https://doi.org/10.3847/1538-4357/acda90

Collinson, G., Wilson, L. B., III., Omidi, N., Sibeck, D., Espley, J., Fowler, C. M., et al. (2018). Solar wind induced waves in the skies of Mars: Ionospheric compression, energization, and escape resulting from the impact of ultralow frequency magnetosonic waves generated upstream of the Martian bow shock. *Journal of Geophysical Research: Space Physics*, *123*(9), 7241–7256. https://doi.org/10.1029/2018JA025414

Connerney, J. E. P., Espley, J., Lawton, P., Murphy, S., Odom, J., Oliversen, R., & Sheppard, D. (2015). The MAVEN magnetic field investigation. *Space Science Reviews*, *195*(1–4), 257–291. https://doi.org/10.1007/s11214-015-0169-4

Cravens, T. E., Fowler, C. M., Brain, D., Rahmati, A., Xu, S., Ledvina, S. A., et al. (2020). Magnetic reconnection in the ionosphere of Mars: The role of collisions. *Journal of Geophysical Research: Space Physics*, *125*(9), e2020JA028036. https://doi.org/10.1029/2020JA028036

Deng, X., & Matsumoto, H. (2001). Rapid magnetic reconnection in the Earth's magnetosphere mediated by whistler waves. *Nature*, *410*(6828), 557–560. https://doi.org/10.1038/35069018

Dong, Y., Fang, X., Brain, D. A., McFadden, J. P., Halekas, J. S., Connerney, J. E., et al. (2015). Strong plume fluxes at Mars observed by MAVEN: An important planetary ion escape channel. *Geophysical Research Letters*, *42*(21), 8942–8950. https://doi.org/10.1002/2015GL065346

Dubinin, E., Fraenz, M., Woch, J., Zhang, T. L., Wei, Y., Fedorov, A., et al. (2013). Toroidal and poloidal magnetic fields at Venus. Venus Express observations. *Planetary and Space Science*, *87*, 19–29. https://doi.org/10.1016/j.pss.2012.12.003

Dubinin, E., Fränz, M., Woch, J., Roussos, E., Barabash, S., Lundin, R., et al. (2006). Plasma morphology at Mars. ASPERA-3 observations. *Space Science Reviews*, *126*(1–4), 209–238. https://doi.org/10.1007/s11214-006-9039-4

Eastwood, J. P., Brain, D. A., Halekas, J. S., Drake, J. F., Phan, T. D., Øieroset, M., et al. (2008). Evidence for collisionless magnetic reconnection at Mars. *Geophysical Research Letters*, *35*(2), L02106. https://doi.org/10.1029/2007GL032289

Eastwood, J. P., Goldman, M. V., Hietala, H., Newman, D. L., Mistry, R., & Lapenta, G. (2015). Ion reflection and acceleration near magnetotail dipolarization fronts associated with magnetic reconnection. *Journal of Geophysical Research: Space Physics*, *120*(1), 511–525. https://doi.org/10.1002/2014JA020516

Fan, K., Wei, Y., Fraenz, M., Cui, J., He, F., Yan, L., et al. (2023). Observations of a mini-magnetosphere above the Martian crustal magnetic fields. *Geophysical Research Letters*, *50*(21), e2023GL103999. https://doi.org/10.1029/2023GL103999

Fowler, C. M., Hanley, K. G., McFadden, J. P., Chaston, C. C., Bonnell, J. W., Halekas, J. S., et al. (2021). MAVEN observations of low frequency steepened magnetosonic waves and associated heating of the Martian nightside ionosphere. *Journal of Geophysical Research: Space Physics*, *126*(10), e2021JA029615. https://doi.org/10.1029/2021JA029615

Gao, J. W., Rong, Z. J., Klinger, L., Li, X. Z., Liu, D., & Wei, Y. (2021). A spherical harmonic Martian crustal magnetic field model combining data sets of MAVEN and MGS. *Earth and Space Science*, *8*(10), e2021EA001860. https://doi.org/10.1029/2021EA001860

Genestreti, K. J., Burch, J. L., Cassak, P. A., Torbert, R. B., Ergun, R. E., Varsani, A., et al. (2017). The effect of a guide field on local energy conversion during asymmetric magnetic reconnection: MMS observations. *Journal of Geophysical Research: Space Physics*, *122*(11), 11–342. https://doi.org/10.1002/2017JA024247

Hapgood, M. A. (1992). Space physics coordinate transformations: A user guide. *Planetary and Space Science*, *40*(5), 711–717. https://doi.org/10.1016/0032-0633(92)90012-D

Harada, Y., Halekas, J. S., DiBraccio, G. A., Xu, S., Espley, J., McFadden, J. P., et al. (2018). Magnetic reconnection on dayside crustal magnetic fields at Mars: MAVEN observations. *Geophysical Research Letters*, *45*(10), 4550–4558. https://doi.org/10.1002/2018GL077281

Harada, Y., Halekas, J. S., McFadden, J. P., Mitchell, D. L., Mazelle, C., Connerney, J. E. P., et al. (2015). Magnetic reconnection in the near-Mars magnetotail: MAVEN observations. *Geophysical Research Letters*, *42*(21), 8838–8845. https://doi.org/10.1002/2015GL065004

Harada, Y., Halekas, J. S., Xu, S., DiBraccio, G. A., Ruhunusiri, S., Hara, T., et al. (2020). Ion jets within current sheets in the Martian magnetosphere. *Journal of Geophysical Research: Space Physics*, *125*(12), e2020JA028576. https://doi.org/10.1029/2020JA028576

Huang, S. Y., Jiang, K., Yuan, Z. G., Sahraoui, F., He, L. H., Zhou, M., et al. (2018). Observations of the Electron jet generated by secondary reconnection in the magnetotail. *The Astrophysical Journal*, *862*(2), 144. https://doi.org/10.3847/1538-4357/aacd4c

Huang, S. Y., Xiong, Q. Y., Song, L. F., Nan, J., Yuan, Z. G., Jiang, K., et al. (2021). Electron-only reconnection in an ion-scale current sheet at the magnetopause. *The Astrophysical Journal*, *922*(1), 54. https://doi.org/10.3847/1538-4357/ac2668

Jiang, K., Huang, S. Y., Yuan, Z. G., Deng, X. H., Wei, Y. Y., Xiong, Q. Y., et al. (2022). Sub-structures of the separatrix region during magnetic reconnection. *Geophysical Research Letters*, *49*(6), e2022GL097909. https://doi.org/10.1029/2022GL097909

Langlais, B., Thébault, E., Houliez, A., Purucker, M. E., & Lillis, R. J. (2019). A new model of the crustal magnetic field of Mars using MGS and MAVEN. *Journal of Geophysical Research: Planets*, *124*(6), 1542–1569. https://doi.org/10.1029/2018JE005854

Liemohn, M. W., Mitchell, D. L., Nagy, A. F., Fox, J. L., Reimer, T. W., & Ma, Y. (2003). Comparisons of electron fluxes measured in the crustal fields at Mars by the MGS Magnetometer/Electron Reflectometer instrument with a B field–dependent transport code. *Journal of Geophysical Research*, *108*(E12), 5134. https://doi.org/10.1029/2003JE002158

Lin, R. T., Huang, S. Y., Yuan, Z. G., Jiang, K., Wu, H. H., & Xiong, Q. Y. (2024). Direct observations of magnetic reconnections at the magnetopause of the Martian mini-magnetosphere. *Geophysical Research Letters*, *51*(13), e2024GL108880. https://doi.org/10.1029/2024GL108880

Lin, R. T., Huang, S. Y., Yuan, Z. G., Jiang, K., Xu, S. B., Wei, Y. Y., et al. (2024). Observation of Interchange reconnection in Mars. *The Astrophysical Journal*, *960*(1), 68. https://doi.org/10.3847/1538-4357/ad0e62

Liu, K., Hao, X., Li, Y., Zhang, T., Pan, Z., Chen, M., et al. (2020). Mars Orbiter magnetometer of China's First Mars Mission Tianwen-1. *Earth and Planetary Physics*, *4*, 384–389. https://doi.org/10.26464/epp2020058

Liu, Y. H., Mouikis, C. G., Kistler, L. M., Wang, S., Roytershteyn, V., & Karimabadi, H. (2015). The heavy ion diffusion region in magnetic reconnection in the Earth's magnetotail. *Journal of Geophysical Research: Space Physics*, *120*(5), 3535–3551. https://doi.org/10.1002/2015JA020982

Ma, X., Tian, A., Guo, R., Chai, L., Shi, Q., Bai, S., et al. (2023). Tianwen-1 and MAVEN observations of Martian oxygen ion plumes. *Icarus*, *406*, 115758. https://doi.org/10.1016/j.icarus.2023.115758

McFadden, J. P., Kortmann, O., Curtis, D., Dalton, G., Johnson, G., Abiad, R., et al. (2015). MAVEN SupraThermal and Thermal Ion Composition (STATIC) instrument. *Space Science Reviews*, *195*(1-4), 199–256. https://doi.org/10.1007/s11214-015-0175-6

Mitchell, D., Lin, R., Reme, H., Crider, D., Cloutier, P., Connerney, J., et al. (2000). Oxygen Auger electrons observed in Mars' ionosphere. *Geophysical Research Letters*, *27*(13), 1871–1874. https://doi.org/10.1029/1999gl010754

Mitchell, D., Mazelle, C., Sauvaud, J. A., Thocaven, J. J., Rouzaud, J., Fedorov, A., et al. (2016). The MAVEN solar wind electron analyzer. *Space Science Reviews*, *200*(1–4), 495–528. https://doi.org/10.1007/s11214-015-0232-1

Modolo, R., Chanteur, G. M., & Dubinin, E. (2012). Dynamic Martian magnetosphere: Transient twist induced by a rotation of the IMF. *Geophysical Research Letters*, *39*(1), L01106. https://doi.org/10.1029/2011GL049895

Phan, T. D., Kistler, L. M., Klecker, B., Haerendel, G., Paschmann, G., Sonnerup, B. U. O., et al. (2000). Extended magnetic reconnection at the Earth's magnetopause from detection of bi-directional jets. *Nature*, *404*(6780), 848–850. https://doi.org/10.1038/35009050

Romanelli, N., DiBraccio, G., Modolo, R., Leblanc, F., Espley, J., Gruesbeck, J., et al. (2019). Recovery timescales of the dayside Martian magnetosphere to IMF variability. *Geophysical Research Letters*, *46*(20), 10977–10986. https://doi.org/10.1029/2019GL084151

Russell, C. T. (2001). Solar wind and interplanetary magnetic field: A tutorial. In P. Song, H. J. Singer, & G. L. Siscoe (Eds.), *Space Weather*. https://doi.org/10.1029/GM125p0073

Shane, A. D., Xu, S., Liemohn, M. W., & Mitchell, D. L. (2016). Mars nightside electrons over strong crustal fields. *Journal of Geophysical Research: Space Physics*, *121*(4), 3808–3823. https://doi.org/10.1002/2015JA021947

Sonnerup, B. U. O. (1979). Magnetic field reconnection. In L. T. Lanzerotti, C. F. Kennel, & E. N. Parker (Eds.), *Solar System plasma physics* (Vol. 3, pp. 47–108).

Sonnerup, B. U. O., & Scheible, M. (1998a). Minimum and maximum variance analysis. In G. Paschmann & P. W. Daly (Eds.), *Analysis methods for multi-spacecraft data, no. SR-001 in ISSI scientific reports Chapter 1* (pp. 185–220). ESA Publications Division.

Sonnerup, B. U. Ö., & Scheible, M. (1998b). Minimum and maximum variance analysis. In G. Paschmann & P. W. Daly (Eds.), *Analysis methods for multi-spacecraft data* (pp. 185–220). International Space Science Institute (ISSI).

Tarduno, J. A., Cottrell, R. D., Watkeys, M. K., Hofmann, A., Doubrovine, P. V., Mamajek, E. E., et al. (2010). Geodynamo, solar wind, and magnetopause 3.4 to 3.45 billion years ago. *Science*, *327*(5970), 1238–1240. https://doi.org/10.1126/science.1183445

Vasyliunas, V. M. (1975). Theoretical models of magnetic field line merging. *Reviews of Geophysics*, *13*(1), 303–336. https://doi.org/10.1029/RG013i001p00303

Vignes, D., Mazelle, C., Rme, H., Acuña, M. H., Connerney, J. E. P., Lin, R. P., et al. (2000). The solar wind interaction with Mars: Locations and shapes of the bow shock and the magnetic pile-up boundary from the observations of the MAG/ER experiment onboard Mars Global Surveyor. *Geophysical Research Letters*, *27*(1), 49–52. https://doi.org/10.1029/1999GL010703

Wang, G. Q., Xiao, S. D., Wu, M. Y., Zhao, Y. D., Jiang, S., Pan, Z. H., et al. (2024). Calibration of the zero offset of the fluxgate magnetometer on board the Tianwen-1 orbiter in the Martian magnetosheath. *Journal of Geophysical Research: Space Physics*, *129*(1), e2023JA031757. https://doi.org/10.1029/2023JA031757

Wang, J., Yu, J., Xu, X., Cui, J., Cao, J., Ye, Y., et al. (2021). MAVEN observations of magnetic reconnection at Martian induced magnetopause. *Geophysical Research Letters*, *48*(21), e2021GL095426. https://doi.org/10.1029/2021GL095426

Wang, Y. M., Zhang, T. L., Wang, G. Q., Xiao, S. D., Zou, Z. X., Cheng, L., et al. (2023). The Mars orbiter magnetometer of Tianwen-1: In-flight performance and first science results. *Earth and Planetary Physics*, *7*(2), 216–228. https://doi.org/10.26464/epp2023028

Weber, T., Brain, D., Mitchell, D., Xu, S., Connerney, J., & Halekas, J. (2017). Characterization of low-altitude nightside Martian magnetic topology using electron pitch angle distributions. *Journal of Geophysical Research: Space Physics*, *122*(10), 9777–9789. https://doi.org/10.1002/2017JA024491

Xiong, Q. Y., Huang, S. Y., Yuan, Z. G., Jiang, K., Lin, R. T., & Yu, L. (2024). Impact of mass-loading effect on the competition in the energy conversion rate during magnetic reconnection. *Journal of Geophysical Research: Space Physics*, *129*(4), e2024JA032470. https://doi.org/10.1029/2024JA032470

Xiong, Q. Y., Huang, S. Y., Yuan, Z. G., Jiang, K., Xu, S. B., Lin, R. T., & Yu, L. (2023). Electron backflow motions in the outer electron diffusion region during magnetic reconnection. *Geophysical Research Letters*, *50*(21), e2023GL105300. https://doi.org/10.1029/2023GL105300

Xu, S., Weber, T., Mitchell, D. L., Brain, D. A., Mazelle, C., DiBraccio, G. A., & Espley, J. (2019). A technique to infer magnetic topology at Mars and its application to the terminator region. *Journal of Geophysical Research: Space Physics*, *124*(3), 1823–1842. https://doi.org/10.1029/2018JA026366

Ye, Y., Xu, X., Lee, L. C., Yu, J., Wang, J., Zhu, B., et al. (2024). In situ observation of mass ejections caused by magnetic reconnections in the ionosphere of Mars. *Nature Astronomy*, *8*(7), 838–845. https://doi.org/10.1038/s41550-024-02254-3

Zenitani, S., Shinohara, I., Nagai, T., & Wada, T. (2013). Kinetic aspects of the ion current layer in a reconnection outflow exhaust. *Physics of Plasmas*, *20*(9), 092120. https://doi.org/10.1063/1.482196

Zhang, C., Nilsson, H., Ebihara, Y., Yamauchi, M., Persson, M., Rong, Z., et al. (2023). Detection of magnetospheric ion drift patterns at Mars. *Nature Communications*, *14*(1), 6866. https://doi.org/10.1038/s41467-023-42630-7

Zomerdijk-Russell, S., Masters, A., Sun, W. J., Fear, R. C., & Slavin, J. A. (2023). Does reconnection only occur at points of maximum shear on Mercury's dayside magnetopause? *Journal of Geophysical Research: Space Physics*, *128*(11), e2023JA031810. https://doi.org/10.1029/2023JA031810

Zou, Z., Wang, Y., Zhang, T., Wang, G., Xiao, S., Pan, Z., et al. (2023). In-flight calibration of the magnetometer on the Mars orbiter of Tianwen-1. *Science China Technological Sciences*, *66*(8), 2396–2405. https://doi.org/10.1007/s11431-023-2401-2